Time-bin entangled photon pairs from spontaneous parametric down-conversion pumped by a cw multi-mode diode laser

Osung Kwon,[1,2,3] **Kwang-Kyoon Park,**[1] **Young-Sik Ra,**[1] **Yong-Su Kim,**[2] **and Yoon-Ho Kim**[1,*]

[1]*Department of Physics, Pohang University of Science and Technology (POSTECH), Pohang, 790-784, South Korea*
[2]*Center for Nano & Quantum Information, Korea Institute of Science and Technology (KIST), Seoul, 136-791, South Korea*
[3]*oskwon98@gmail.com*

[*]*yoonho72@gmail.com*

Abstract: Generation of time-bin entangled photon pairs requires the use of the Franson interferometer which consists of two spatially separated unbalanced Mach-Zehnder interferometers through which the signal and idler photons from spontaneous parametric down-conversion (SPDC) are made to transmit individually. There have been two SPDC pumping regimes where the scheme works: the narrowband regime and the double-pulse regime. In the narrowband regime, the SPDC process is pumped by a narrowband cw laser with the coherence length much longer than the path length difference of the Franson interferometer. In the double-pulse regime, the longitudinal separation between the pulse pair is made equal to the path length difference of the Franson interferometer. In this paper, we propose another regime by which the generation of time-bin entanglement is possible and demonstrate the scheme experimentally. In our scheme, differently from the previous approaches, the SPDC process is pumped by a cw multi-mode (i.e., short coherence length) laser and makes use of the coherence revival property of such a laser. The high-visibility two-photon Franson interference demonstrates clearly that high-quality time-bin entanglement source can be developed using inexpensive cw multi-mode diode lasers for various quantum communication applications.

References and links

1. J. P. Dowling and G. J. Milburn, "Quantum technology: the second quantum revolution," Phil. Trans. R. Soc. Lond. A **361**, 1655-1674 (2003).
2. M. A. Nielsen and I. L. Chuang, *Quantum Computation and Quantum Information* (Cambridge University, 2000).
3. A. K. Ekert, "Quantum cryptography based on Bell's theorem," Phys. Rev. Lett. **67**, 661–663 (1991).
4. C. H. Bennett, G. Brassard, C. Crépeau, R. Jozsa, A. Peres, and W. K. Wootters, "Teleporting an unknown quantum state via dual classical and Einstein-Podolsky-Rosen channels," Phys. Rev. Lett. **70**, 1895–1899 (1993).
5. D. Bouwmeester, J.-W. Pan, K. Mattle, M. Eibl, H. Weinfurter, and A. Zeilinger, "Experimental quantum teleportation," Nature **390**, 575–579 (1997).

6. Y.-H. Kim, S. P. Kulik, and Y. Shih, "Quantum teleportation of a polarization state with a complete Bell state measurement," Phys. Rev. Lett. **86**, 1370–1373 (2001).

7. V. Giovannetti, S. Lloyd, and L. Maccone, "Advances in quantum metrology," Nat. Photonics **5**, 222–229 (2011).

8. O. Kwon, Y.-S. Ra, and Y.-H. Kim, "Observing photonic de Broglie waves without the maximally-path-entangled $|N,0\rangle + |0,N\rangle$ state," Phys. Rev. A **81**, 063801 (2010).

9. Y.-S. Ra, M. C. Tichy, H.-T. Lim, O. Kwon, F. Mintert, A. Buchleitner, and Y.-H. Kim, "Observation of detection-dependent multi-photon coherence times," Nature Commun. **4**, 2451 (2013).

10. Y. H. Shih and C. O. Alley, "New type of Einstein-Podolsky-Rosen-Bohm experiment using pairs of light quanta produced by optical parametric down conversion," Phys. Rev. Lett. **61**, 2921–2924 (1988).

11. Z. Y. Ou and L. Mandel, "Violation of Bell's inequality and classical probability in a two-photon correlation experiment," Phys. Rev. Lett. **61**, 50–53 (1988).

12. P. G. Kwiat, K. Mattle, H. Weinfurter, A. Zeilinger, A.V. Sergienko, and Y. Shih "New high-intensity source of polarization-entangled photon pairs," Phys. Rev. Lett. **75**, 4337–4341 (1995).

13. H.-T. Lim, Y.-S. Kim, Y.-S. Ra, J. Bae, and Y.-H. Kim, "Experimental realization of an approximate partial transpose for photonic two-qubit systems," Phys. Rev. Lett. **107**, 160401 (2011).

14. Y.-S. Kim, J.-C. Lee, O. Kwon, and Y.-H. Kim, "Protecting entanglement from decoherence using weak measurement and quantum measurement reversal," Nature Phys. **8**, 117–120 (2012).

15. R. T. Thew, S. Tanzilli, W. Tittel, H. Zbinden, and N. Gisin, "Experimental investigation of the robustness of partially entangled qubits over 11 km," Phys. Rev. A **66**, 062304 (2002).

16. J. F. Dynes, H. Takesue, Z. L. Yuan, A. W. Sharpe, K. Harada, T. Honjo, H. Kamada, O. Tadanaga, Y. Nishida, M. Asobe, and A. J. Shields, "Efficient entanglement distribution over 200 kilometers," Opt. Express **17**, 11440–11449 (2009).

17. J. D. Franson, "Bell inequality for position and time," Phys. Rev. Lett. **62**, 2205–2208 (1989).

18. J. Brendel, E. Mohler, and W. Martienssen, "Time-resolved dual-beam two-photon interferences with high visibility," Phys. Rev. Lett. **66**, 1142–1145 (1991).

19. J. G. Rarity and P. R. Tapster, "Fourth-order interference effects at large distances," Phys. Rev. A **45**, 2052–2056 (1992).

20. Y. H. Shih, A. V. Sergienko, and M. H. Rubin, "Einstein-Podolsky-Rosen state for space-time variables in a two-photon interference experiment," Phys. Rev. A **47**, 1288–1293 (1993).

21. P. G. Kwiat, A. M. Steinberg, and R. Y. Chiao, "High-visibility interference in a Bell-inequality experiment for energy and time," Phys. Rev. A **47**, R2472–R2475 (1993).

22. D. V. Strekalov, T. B. Pittman, A. V. Sergienko, Y. H. Shih, and P. G. Kwiat, "Postselection-free energy-time entanglement," Phys. Rev. A **54**, R1–R4 (1996).

23. T. Honjo, H. Takesue, and K. Inoue, "Generation of energy-time entangled photon pairs in 1.5-μm band with periodically poled lithium niobate waveguide," Opt. Express **15**, 1679–1683 (2007).

24. J. Brendel, N. Gisin, W. Tittel, and H. Zbinden, "Pulsed energy-time entangled twin-photon source for quantum communication," Phys. Rev. Lett. **82**, 2594–2597 (1999).

25. W. Tittel, J. Brendel, H. Zbinden, and N. Gisin, "Quantum cryptography using entangled photons in energy-time Bell states," Phys. Rev. Lett. **84**, 4737–4740 (2000).

26. I. Marcikic, H. de Riedmatten, W. Tittel, V. Scarani, H. Zbinden, and N. Gisin, "Time-bin entangled qubits for quantum communication created by femtosecond pulses," Phys. Rev. A **66**, 062308 (2002).

27. W. Tittel, J. Brendel, H. Zbinden, and N. Gisin, "Violation of Bell inequalities by photons more than 10 km apart," Phys. Rev. Lett. **81**, 3563–3566 (1998).

28. A. V. Burlakov, M. V. Chekhova, O. A. Karabutova, and S. P. Kulik, "Biphoton interference with a multimode pump," Phys. Rev. A **63**, 053801 (2001).

29. S.-Y. Baek, O. Kwon, and Y.-H. Kim, "High-resolution mode-spacing measurement of the blue-violet diode lase using interference of fields created with time delays greater than the coherence time," Jpn. J. Appl. Phys. **46**, 7720–7723 (2007).

30. O. Kwon, Y.-S. Ra, and Y.-H. Kim, "Coherence properties of spontaneous parametric down-conversion pumped by a multi-mode cw diode laser," Opt. Express **17**, 13059–13069 (2009).

31. J. F. Clauser and M. A. Horne, "Experimental consequences of objective local theories," Phys. Rev. D **10**, 526–535 (1974).

32. J. Galinis, M. Karpiński, G. Tamošauskas, K. Dobek, and A. Piskarskas, "Photon coincidences in spontaneous parametric down-converted radiation excited by a blue LED in bulk LiIO3 crystal," Opt. Express **19**, 10351–10358 (2011).

1. Introduction

Entanglement is one of the most fascinating non-classical properties [1]. It is also a very important resource for many quantum information applications such as quantum computation [2], quantum cryptography [3], quantum teleportation [4–6], and quantum metrology [7–9].

For photons, polarization-entanglement [10–12] is widely utilized in quantum information research [13, 14], but it is not ideal for fiber-based quantum communication applications due to the polarization mode dispersion. Time-bin entanglement is often the best choice for such applications as it is robust against various decoherence effects resulting from long-distance fiber transmission [15, 16].

The generation scheme for time-bin entanglement is based on the Franson interferometer (FI) [17], which consists of two spatially separated unbalanced Mach-Zehnder interferometers through which the signal and idler photons from spontaneous parametric down-conversion (SPDC) are made to transmit individually, see Fig. 1. In quantum interference experiments, it is essential to ensure that the relevant quantum probability amplitudes are made indistinguishable and in the experiments involving the FI, this is achieved by choosing proper pumping schemes. There have been two SPDC pumping regimes where the scheme works: the narrowband regime and the double-pulse regime. In the narrowband regime [18–23], the SPDC process is pumped by a narrowband cw laser with the coherence length much longer than the path length difference of the FI. In the double-pulse regime [24–27], the longitudinal separation between the pulse pair is made equal to the path length difference of the FI.

In this paper, we propose another regime by which the generation of time-bin entanglement is possible and demonstrate the scheme experimentally. In our scheme, differently from the previous approaches, the SPDC process is pumped by a cw multi-mode (i.e., short coherence length) laser. By making use of the coherence revival property of a cw multi-mode laser, observed for the first-order coherence in [28, 29] and for the second-order coherence in [30], we demonstrate high-visibility quantum interference due to two-photon energy-time entanglement. Our results clearly show that high-quality time-bin entanglement source can be developed using inexpensive cw multi-mode diode lasers, as opposed to using expensive narrowband lasers or pulsed lasers, for various quantum communication applications.

2. Theory

We begin by briefly introducing the Franson interferometer shown in Fig. 1 [17]. A pair of photons, typically called the signal and the idler photons, are generated from the SPDC process in a nonlinear crystal. Each photon is directed to an unbalanced Mach-Zehnder interferometer (MZI) and the photon may take the long path (L_1 and L_2) or the short path (S_1 and S_2) of the MZI. To ensure that there is no first-order interference at the output of the MZI, the path length difference between the long path and the short path is made much larger than the coherence
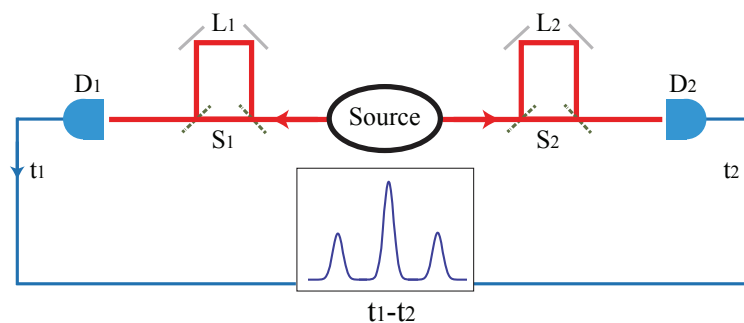

Fig. 1. The schematic of Franson interferometer. Post-selecting the central peak in the TC-SPC histogram allows one to prepare/detect the time-bin entanglement. For this to happen, the pump laser for the SPDC process must meet certain conditions. See text for details.

length of the input (signal and idler) photon. The photons are then detected at the single-photon detectors (D_1 and D_2) located at the output ports of the MZI and the difference of photons' time of arrival $\tau = t_1 - t_2$ is recorded by using Time-Correlated Single-Photon Counting (TCSPC) electronics.

It is well-known that the TCSPC histogram exhibits three distinctive peaks as shown in Fig. 1 and they come from the four probability amplitudes for joint detection of the photon pair: $|S\rangle_1 |S\rangle_2$, $|L\rangle_1 |L\rangle_2$, $|S\rangle_1 |L\rangle_2$, and $|L\rangle_1 |S\rangle_2$. The left (right) peak is due to $|S\rangle_1 |L\rangle_2$ ($|L\rangle_1 |S\rangle_2$) and the central peak is due to both $|S\rangle_1 |S\rangle_2$ and $|L\rangle_1 |L\rangle_2$ which is why the central peak is twice as tall as the side peaks. Note that the separation between peaks is determined by the optical path length difference of the MZI $\Delta L_{1,2} = L_{1,2} - S_{1,2}$ and the width of the peak (typically around $1 \sim 2$ ns) is mostly determined by the resolution of the electronics. Since $L_c \ll \Delta L_{1,2}$, where L_c is the coherence length of the single-photons (signal and idler photons), there is no first-order interference observed at either detectors D_1 and D_2. We then further impose the condition $\Delta L_{1,2} \ll L_p$, where L_p is the coherence length of the SPDC pump laser, and post-select only the central peak of the TCSPC histogram by using a narrow coincidence window. We have thus obtained a time-bin entangled state

$$|\psi\rangle = \frac{1}{\sqrt{2}}(|S\rangle_1 |S\rangle_2 + e^{i\phi} |L\rangle_1 |L\rangle_2), \tag{1}$$

where ϕ is the phase difference between two probability amplitudes, which can be controlled by scanning $\Delta L_{1,2}$ of the MZI. The visibility drops if the side peaks are not completely excluded.

The description so far is the narrowband regime as the pump bandwidth should be sufficiently narrow to satisfy $\Delta L_{1,2} \ll L_p$, which is essential for providing quantum coherence between $|S\rangle_1 |S\rangle_2$ and $|L\rangle_1 |L\rangle_2$ [18–23]. Another way to ensure quantum coherence between the two amplitudes $|S\rangle_1 |S\rangle_2$ and $|L\rangle_1 |L\rangle_2$ is to pump the SPDC process with a pair of coherent pulses, the double-pulse regime, whose longitudinal separation is identical to $\Delta L_{1,2}$ [24–27]. Unlike these schemes, our new scheme for generating time-bin entanglement does not use the narrowband pumping nor coherent pulses. In fact, the pump laser in our scheme has a coherence length much smaller than the path length difference of the MZI, $L_p \ll \Delta L_{1,2}$. Instead, our scheme is based on the coherence revival property of multi-mode emission from a cavity [28–30].

Let us begin by describing the SPDC process pumped by a multi-mode laser. The two-photon state from multi-mode pumped SPDC can be written as a mixed state [8, 30]

$$\rho = \int d\omega_p \mathscr{S}(\omega_p) |\psi\rangle\langle\psi|. \tag{2}$$

Here, $\mathscr{S}(\omega_p)$ is the spectral power density of the pump laser given as the sum of multiple incoherent longitudinal modes,

$$\mathscr{S}(\omega_p) = \frac{\sum_{n=-N}^{N} \mathscr{S}_0(\omega_p) \delta(\omega_p - \omega_{p0} - n\Delta\omega_p)}{\sum_{n=-N}^{N} \mathscr{S}_0(\omega_{p0} + n\Delta\omega_p)}, \tag{3}$$

where ω_{p0}, $\Delta\omega_p$, and n are the central frequency of the pump, the mode spacing, and the mode number and we have assumed that the spectral power density has a Gaussian spectral profile with the bandwidth θ, $\mathscr{S}_0(\omega_p) \sim \exp\left[-\frac{(\omega_p - \omega_{p0})^2}{2\theta^2}\right]$. The two-photon quantum state of SPDC $|\psi\rangle$, pumped by a single-mode laser with frequency ω_p is given as

$$|\psi\rangle = \int d\omega_s d\omega_i \, \delta(\Delta_\omega) \mathrm{sinc}(\Delta_k l/2) e^{i\Delta_k l/2} |\omega_s, \omega_i\rangle, \tag{4}$$

where $\Delta_\omega \equiv \omega_p - \omega_s - \omega_i$, $\Delta_k \equiv k_p - k_s - k_i$, and l is the thickness of the SPDC crystal. The subscripts p, s, and i refer the pump, signal, and idler photons, respectively. Note that $|\omega_s, \omega_i\rangle =$

$a_s^\dagger(\omega_s)a_i^\dagger(\omega_i)|0\rangle$ where $a_s^\dagger(\omega_s)$ ($a_i^\dagger(\omega_i)$) represents the creation operator for the signal (idler) photon of frequency ω_s (ω_i) and $|0\rangle$ is the vacuum.

Let us now suppose that the signal (idler) photon is sent to D_1 (D_2) through the unbalanced MZIs in Fig. 1. We also assume that interference filters are placed in front of the detectors and they have the Gaussian transmission function $\phi(\omega) = \frac{1}{\sqrt{\theta_f\sqrt{\pi}}}\exp\left[-\frac{(\omega-\omega_0)^2}{2\theta_f^2}\right]$, where ω_0 and θ_f are the central frequency and bandwidth of the filter, respectively, and $\int|\phi(\omega)|^2 d\omega = 1$. Consequently, the positive frequency component of the electric field operator for a single-photon detector $D_{j\in\{1,2\}}$ at time t is expressed as $E_{D_j}^{(+)}(t) = \int d\omega\ \phi(\omega)e^{-i\omega t}a_{D_j}(\omega)$, where $a_{D_j}(\omega)$ is the annihilation operator for a photon of frequency ω at the detector D_j.

The joint detection rate between the two detectors D_1 and D_2 is then proportional to

$$R \propto \int_{-\Delta\tau}^{\Delta\tau} d\tau\ tr[\rho E_{D_1}^{(-)}(t)E_{D_2}^{(-)}(t+\tau)E_{D_2}^{(+)}(t+\tau)E_{D_1}^{(+)}(t)], \tag{5}$$

where $E_{D_{j\in\{1,2\}}}^{(+)}(t) = \frac{1}{\sqrt{2}}\left[E_{S_j}^{(+)}(t)+E_{L_j}^{(+)}(t-\xi_j)\right]$, $\xi_j = \Delta L_j/c$ with c being the speed of light in vacuum, and $\tau = t_1 - t_2$. In evaluating the integral in Eq. (5), we set the value of $\Delta\tau$ such that only the central peak in the TCSPC histogram (see Fig. 1) is selected (i.e., two side peaks are thrown out). Thus, the field operator $E_{D_2}^{(+)}(t+\tau)E_{D_1}^{(+)}(t)$ becomes $\frac{1}{2}\left[E_{S_2}^{(+)}(t+\tau)E_{S_1}^{(+)}(t)+E_{L_2}^{(+)}(t+\tau-\xi_2)E_{L_1}^{(+)}(t-\xi_1)\right]$ without containing the terms representing the side peaks $E_{S_2}^{(+)}E_{L_1}^{(+)}$ and $E_{L_2}^{(+)}E_{S_1}^{(+)}$. Therefore, Eq. (5) becomes

$$R \propto \int d\tau\ tr\left[\rho\left(E_{S_2}^{(-)}(t+\tau)E_{S_1}^{(-)}(t)+E_{L_2}^{(-)}(t+\tau-\xi_2)E_{L_1}^{(-)}(t-\xi_1)\right)\right.$$
$$\left.\times\left(E_{S_2}^{(+)}(t+\tau)E_{S_1}^{(+)}(t)+E_{L_2}^{(+)}(t+\tau-\xi_2)E_{L_1}^{(+)}(t-\xi_1)\right)\right]. \tag{6}$$

Considering the fact that the signal (idler) photon propagates toward D_1 (D_2) and given that the field operators for the signal and the idler photons are given as $E_j^{(+)}(t) = \int d\omega\ \phi(\omega)e^{-i\omega t}a_j(\omega)$ with $j \in \{s,i\}$, we can write $E_{S_1}^{(+)}(t) = \frac{1}{\sqrt{2}}E_s^{(+)}(t)$, $E_{S_2}^{(+)}(t) = \frac{1}{\sqrt{2}}E_i^{(+)}(t)$, and similarly for $E_{L_1}^{(+)}(t)$ and $E_{L_2}^{(+)}(t)$. After substituting Eq. (2) for ρ in Eq. (6), we finally obtain the joint detection rate

$$R = \frac{1}{2} + \frac{\Gamma}{2}\frac{\sum_{n=-N}^{N}\mathscr{S}_{\text{eff}}(\omega_{p0}+n\Delta\omega_p)\cos\left((\omega_{p0}+n\Delta\omega_p)(\xi_1+\xi_2)\right)}{\sum_{n=-N}^{N}\mathscr{S}_{\text{eff}}(\omega_{p0}+n\Delta\omega_p)}, \tag{7}$$

where $\Gamma = \exp\left[-\theta_f^2(\xi_1-\xi_2)^2/8\right]$ and $\mathscr{S}_{\text{eff}}(\omega_p)$ identical to $\mathscr{S}_0(\omega_p)$ except that the bandwidth θ is replaced with the effective bandwidth θ_{eff} (calculated from $1/\theta_{\text{eff}}^2 = 1/\theta^2 + 1/\theta_f^2$). We have assumed that the filter bandwidth θ_f is sufficiently narrower than the natural bandwidth of SPDC (calculated from $\text{sinc}(\Delta_k l/2)$) so that the SPDC spectral amplitude is equal to the filter transmission function $\phi(\omega)$.

Figure 2 shows the theoretical results of Eq. (7). Here we have assumed that the multi-mode pump laser is centered at $\lambda_{p0} = 405$ nm with the bandwidth of $\sigma = 0.28$ nm and the mode spacing is $\Delta\lambda_p = 0.0289$ nm. The SPDC photons are assumed to be generated at a type-I BBO crystal of thickness $l = 6$ mm and centered at $\lambda_0 = 810$ nm. The bandwidth of the filter transmission function is assumed to be $\sigma_f = 17$ nm. These parameters are converted to frequencies by using the following relations $\omega_0 = 2\pi c/\lambda_0$, $\theta = 2\pi c\sigma/\lambda_0^2$, and $\Delta\omega_p = 2\pi c\Delta\lambda_p/\lambda_{p0}^2$. Note that, at these conditions, the multi-mode pump laser exhibits the coherence revival at the period of $L_r = \lambda_{p0}^2/\Delta\lambda_p = 5.668$ mm [29, 30].
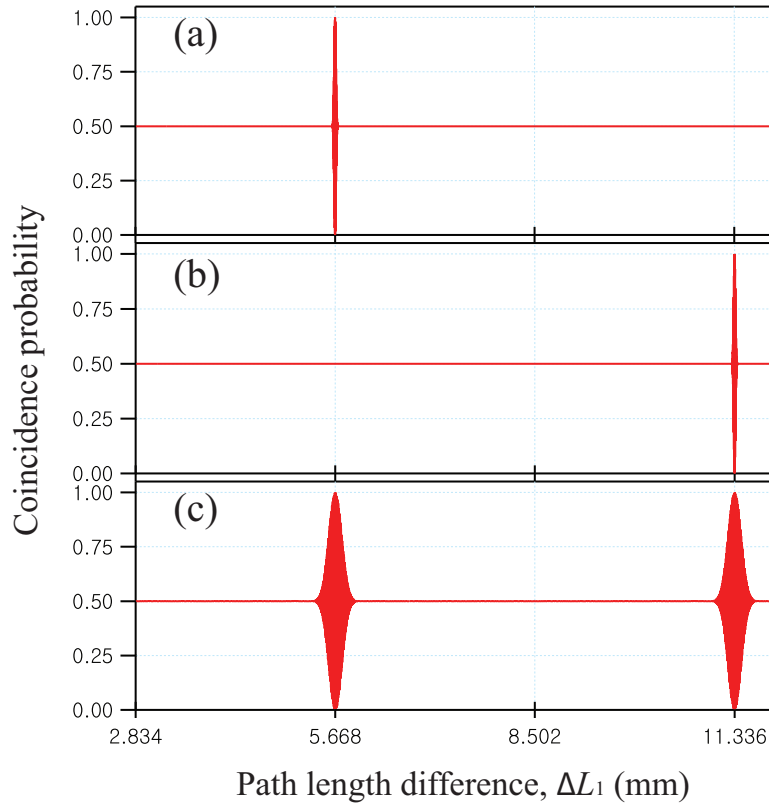
Fig. 2. Theoretical plot of Eq. (7) as a function of ΔL_1 for different ΔL_2. (a) $\Delta L_2 = 5.668$ mm and (b) $\Delta L_2 = 11.336$ mm. (c) The joint count rate when ΔL_1 and ΔL_2 are simultaneously scanned exhibits the coherence revival property [29, 30].

We first consider the cases where one of the MZIs is unbalanced at integer multiples of L_r. Figures 2(a) and 2(b) show the coincidence rates as a function of ΔL_1, while ΔL_2 is fixed at L_r and $2L_r$, respectively. As demonstrated in the theoretical plots, two-photon time-bin interference fringes are expected whenever the scanning ΔL_1 becomes identical to ΔL_2 within the single-photon coherence length. It is important to point out that, since the individual MZI is unbalanced, there is no first-order interference. Note also that, in this case, the interference fringes exhibit modulation at the wavelength of SPDC photons $\lambda_0 = 810$ nm. Consider now that both ΔL_1 and ΔL_2 are scanned simultaneously shown in Fig. 2(c). In this case, two-photon interference is expected at the modulation period equal to the pump wavelength $\lambda_{p0} = 405$ nm. Furthermore, coherence revival of the two-photon time-bin interference fringes is expected at the period of $L_r = \lambda_{p0}^2/\Delta\lambda_p = 5.668$ mm [29, 30] which is due to the fact that $\Gamma = \exp\left[-\theta_f^2(\xi_1 - \xi_2)^2/8\right]$ in Eq. (7) is not degraded as long as $\Delta L_1 = \Delta L_2$. However, if ΔL_1 differs significantly from ΔL_2, Γ degrades quickly so the revival of two-photon interference does not occur as shown in Figs. 2(a) and 2(b).

3. Experiment

To demonstrate high-visibility two-photon quantum interference due to time-bin entanglement using the multi-mode pump laser, it is essential that the path length differences of the MZIs are set integer multiples of L_r and the side peaks due to $|S\rangle_1|L\rangle_2$ and $|S\rangle_2|L\rangle_1$ are sufficiently
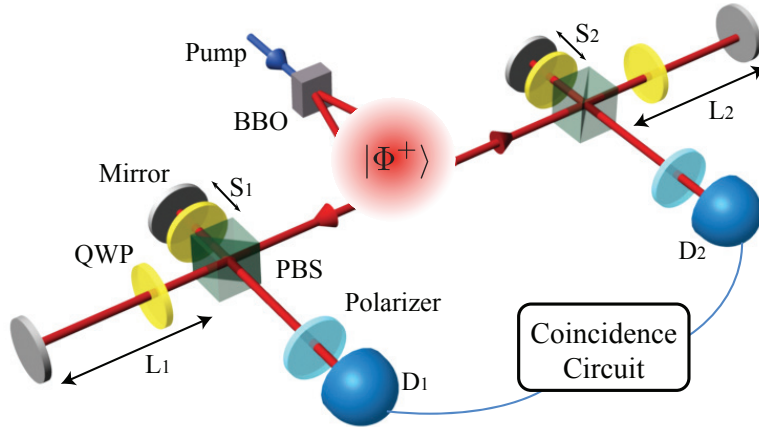
Fig. 3. Experimental setup. PBS: polarization beam splitter, QWP: quarter wave plate, D_1 and D_2: single photon detectors.

far away from the main peak. Considering the detector jitter and TCSPC electronics resolution, about 3 ns separation is desired and this translates to $\Delta L_{1,2} = 900$ mm. To avoid practical problems involving MZIs with such a large path length difference while still demonstrating the essential features of time-bin entanglement using multi-mode pumped SPDC, we employ the postselection-free energy-time entanglement scheme in [22]. In this scheme, beam splitters in the MZIs are replaced with polarization beam splitters and the input state is given in the form of a polarization entangled state. As a result, the $|S\rangle_1|L\rangle_2$ and $|S\rangle_2|L\rangle_1$ amplitudes which generate the side peaks do not occur naturally and therefore no postselection is necessary. Note however that, since the photonic path (long and short) is correlated to the polarization (vertical and horizontal), it is necessary to erase the polarization information by projecting it onto the 45° oriented polarizers [22].

The experimental setup is shown in Fig. 3. Type-I SPDC photon pairs generated in a 6-mm-thick β-BaB$_2$O$_4$ crystal pumped by a 405 nm multi-mode diode laser are used for the experiment. For the 405 nm pump laser, the coherence length and the first-order coherence revival period are measured as $L_p = 216$ μm and $L_r = 5.668$ mm, respectively. From these results, we can find that the mode spacing of the pump laser is $\Delta\omega_p = 3.33 \times 10^{11}$ Hz as simulated in the previous section. The degenerate phase matching condition was applied for the SPDC so the wavelengths of both signal and idler SPDC photons are centered at 810 nm.

First, the polarization entangled state of the form $|\Phi^+\rangle = \frac{1}{\sqrt{2}}(|H\rangle_1|H\rangle_2 + |V\rangle_1|V\rangle_2)$, where $|H\rangle$ and $|V\rangle$ are horizontal and vertical polarization, is prepared by interfering the two photons at a beam splitter [10, 11]. Second, each photon of the polarization entangled state is sent to a unbalanced Michelson interferometer which consists of a polarizing beam splitter (PBS) and two quarter wave plates (QWP). This scheme ensures that the $|H\rangle$ photon at the input of the PBS takes the long path ($|L\rangle_1$ or $|L\rangle_2$) of the interferometer and exits the PBS as the $|V\rangle$ photon. Similarly, $|V\rangle$ photon at the input of the PBS takes the short path ($|S\rangle_1$ or $|S\rangle_2$) of the interferometer and exits the PBS as the $|H\rangle$ photon. Finally, 45° oriented polarizers are used to erase the polarization information. As a result, the polarization-entangled state has been converted to the time-bin entangled state of the form in Eq. (1) with no need for TCSPC postselection. Note that the relative phase ϕ can be adjusted by scanning either ΔL_1 or ΔL_2.

The experimental data are shown in Fig. 4. Figures 4(a) and 4(b) show the coincidence count rate as a function of ΔL_1 while ΔL_2 is fixed at 5.668 mm and 11.336 mm, respectively. As
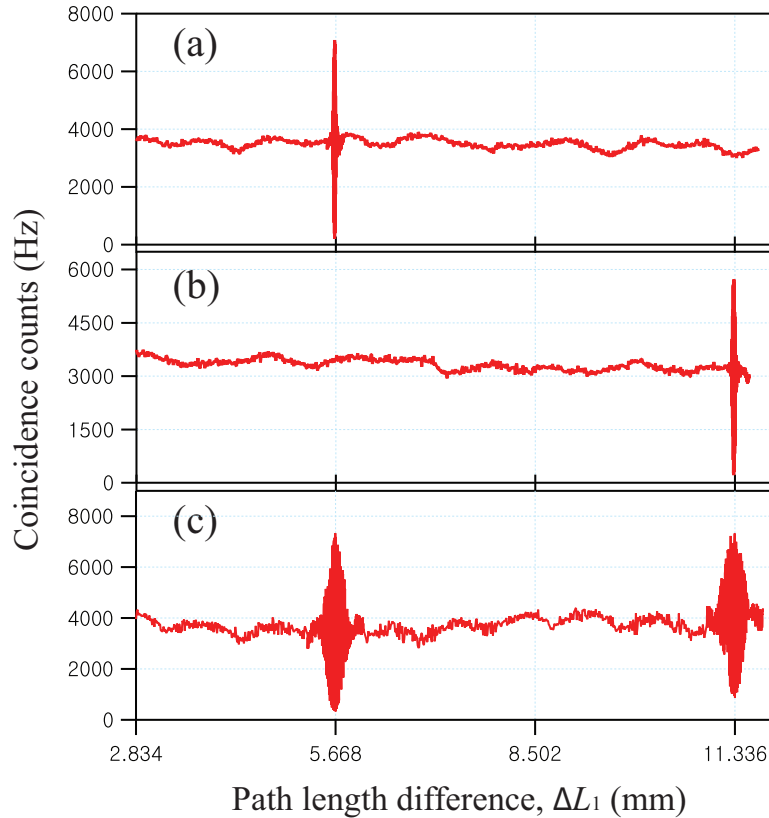
Fig. 4. Experimental data. The coincidence count rate as a function of ΔL_1 for different ΔL_2 values. (a) $\Delta L_2 = 5.668$ mm and (b) $\Delta L_2 = 11.336$ mm. The two-photon interference visibility is measure to be 95% for both cases. (c) ΔL_1 and ΔL_2 are scanned simultaneously. The two-photon interference visibility is measured to be 93%. The experimental data agree well with the theoretical results shown in Fig. 2.

expected in Eq. (7) and in Figs. 2(a) and 2(b), two-photon quantum interference due to time-bin entanglement occurs only when the condition $\Delta L_1 = \Delta L_2$ is satisfied. Figure 4(c) shows the coincidence count rate when both ΔL_1 and ΔL_2 are simultaneously scanned. In this case, as expected in Fig. 2(c), recurrence or revival of two-photon interference is observed with the period of 5.668 mm. The observed quantum interference visibilities are 95% for Fig. 4(a) and 4(b) and 93% for Fig. 4(c). Since the visibility threshold for the two-photon quantum interference for the Bell's inequality violation is 70.7% [31], the experimental data in Fig. 4 show that the photon pair is time-bin entangled, hence suitable for a variety of quantum communications applications.

4. Conclusion

We have shown in theory and in experiment that time-bin entangled photon pairs can be generated with the SPDC process pumped with a cw multi-mode laser. Unlike previous schemes where the pump laser must have coherence length longer than the path length difference of the ranson interferometer [18–23] or the SPDC process must be pumped with a pair of coherent laser pulses whose spatial separation is equal to the path length difference of the Franson interferometer [24–27], our scheme makes use of a unique coherence revival property of the cw

multi-mode laser for generating a time-bin entangled photon pair [28–30]. Clearly, the main difference between the multi-mode cw laser and the mode-locked pulsed laser is the lack of or presence of coherence among the spectral modes. This point is clearly described in Eq. (3) in which the spectral power density of the cw multi-mode laser is given as the incoherent sum of multiple equally-spaced longitudinal modes. We have shown that it is nevertheless possible to use such a laser in the Franson interferometer to prepare time-bin entangled photon pairs. Note that the coherence revival feature of the pump laser, which we make use of for generating the two-photon time-bin entanglement, comes from the fact that the spectral modes are equally-spaced albeit with no phase coherence. Thus, our scheme is not applicable to SPDC pumped with a chaotic light source, e.g, a blue light emitting diode [32].

As multi-mode diode lasers suitable for SPDC pumping are widely available at a low cost, we believe our results offer a wide variety of applications in preparing time-bin entangled photon pairs inexpensively and reliably for various quantum information tasks, such as quantum cryptography, quantum communication, and quantum computation.